Published in final edited form as:
Cell Mol Life Sci. 2013 August ; 70(15): 2757–2771. doi:10.1007/s00018-013-1284-6.

TRPM7 is regulated by halides through its kinase domain

Haijie Yu,
Center for Biomedical Research, The Queen's Medical Center, 1301 Punchbowl St., Honolulu, HI 96813, USA; University of Hawaii Cancer Center & John A. Burns School of Medicine, University of Hawaii, Honolulu, HI 96813, USA

Zheng Zhang,
Center for Biomedical Research, The Queen's Medical Center, 1301 Punchbowl St., Honolulu, HI 96813, USA; University of Hawaii Cancer Center & John A. Burns School of Medicine, University of Hawaii, Honolulu, HI 96813, Usa

Annette Lis,
Center for Biomedical Research, The Queen's Medical Center, 1301 Punchbowl St., Honolulu, HI 96813, USA; University of Hawaii Cancer Center & John A. Burns School of Medicine, University of Hawaii, Honolulu, HI 96813, USA

Reinhold Penner, and
Center for Biomedical Research, The Queen's Medical Center, 1301 Punchbowl St., Honolulu, HI 96813, USA; University of Hawaii Cancer Center & John A. Burns School of Medicine, University of Hawaii, Honolulu, HI 96813, USA

Andrea Fleig
Center for Biomedical Research, The Queen's Medical Center, 1301 Punchbowl St., Honolulu, HI 96813, USA; University of Hawaii Cancer Center & John A. Burns School of Medicine, University of Hawaii, Honolulu, HI 96813, USA

Abstract

Transient receptor potential melastatin 7 (TRPM7) is a divalent-selective cation channel fused to an atypical α-kinase. TRPM7 is a key regulator of cell growth and proliferation, processes accompanied by mandatory cell volume changes. Osmolarity-induced cell volume alterations regulate TRPM7 through molecular crowding of solutes that affect channel activity, including magnesium (Mg^{2+}), Mg-nucleotides and a further unidentified factor. Here, we assess whether chloride and related halides can act as negative feedback regulators of TRPM7. We find that chloride and bromide inhibit heterologously expressed TRPM7 in synergy with intracellular Mg^{2+} ($[Mg^{2+}]_i$) and this is facilitated through the ATP-binding site of the channel's kinase domain. The synergistic block of TRPM7 by chloride and Mg^{2+} is not reversed during divalent-free or acidic conditions, indicating a change in protein conformation that leads to channel inactivation. Iodide has the strongest inhibitory effect on TRPM7 at physiological $[Mg^{2+}]_i$. Iodide also inhibits endogenous TRPM7-like currents as assessed in MCF-7 breast cancer cells, where upregulation of SLC5A5 sodium-iodide symporter enhances iodide uptake and inhibits cell proliferation. These results indicate that chloride could be an important factor in modulating TRPM7 during osmotic

A. Fleig (✉) afleig@hawaii.edu.
Present Address: A. Lis Institute of Biophysics, University of Homburg, 66421 Homburg, Germany
H. Yu and Z. Zhang contributed equally to this work.

Conflict of interests All authors declare no conflict of interests.

Electronic supplementary material The online version of this article (doi:10.1007/s00018-013-1284-6) contains supplementary material, which is available to authorized users.

stress and implicate TRPM7 as a possible molecular mechanism contributing to the anti-proliferative characteristics of intracellular iodide accumulation in cancer cells.

Keywords

TRPM7-inhibitor; Chloride; Iodide; Cell proliferation; Breast cancer

Introduction

TRPM7 is a member of the melastatin-like transient receptor potential (TRPM) subfamily. This protein possesses both an ion channel and a functional serine/threonine α-kinase domain. TRPM7 is unique in that it provides cellular influx for calcium (Ca^{2+}), magnesium (Mg^{2+}), and divalent trace metals [1–3]. The protein is critical for Mg^{2+} regulation of mammalian organisms, with the channel domain facilitating cellular Mg^{2+} influx and the kinase domain regulating Mg^{2+} absorption [4]. TRPM7 activity is inhibited by intracellular Mg^{2+} and also directly linked to the energy status of a cell, since the channel is strongly suppressed in the presence of physiological amounts of Mg·ATP [3, 5, 6]. While the kinase domain is dispensable for TRPM7's channel function, it is involved in the modulation of channel activity [7–9]. Loss of kinase activity decreases the channel's sensitivity to intracellular Mg^{2+} and Mg·ATP, whereas deletion of the kinase domain beyond amino acid 1569 enhances Mg^{2+} inhibition [7]. Thus it has been postulated that the TRPM7 protein has two Mg^{2+} binding sites, one on the kinase domain corresponding with the Mg·nucleotide binding site, and one as yet unidentified site on the channel proper [7]. In addition to Mg^{2+} and Mg·ATP, TRPM7 channel activity is regulated by other secondary messengers such as polyvalent ions [10], pH [10, 11], extracellular divalents [3, 12, 13], PIP_2 [14], and cAMP [15]. The closest protein to TRPM7 in structure is TRPM6. Like TRPM7, TRPM6 is thought to be involved in Mg^{2+} transport, since mutations in the gene were found responsible for an autosomal recessive form of familial hypomagnesemia with secondary hypocalcemia [16, 17]. However, unlike the ubiquitously expressed TRPM7, TRPM6 expression is more limited and found pre-dominantly in colon and kidney epithelia.

TRPM7 has been implicated to be a regulator of cell proliferation [18–21], inducing cell cycle arrest when blocked. This is based on the channel's function in Mg^{2+} transport, since cell growth can be restored by Mg^{2+} supplementation [3, 4, 7, 20, 22, 23]. TRPM7 is involved in cell cycle progression at the G1 phase in rat basophilic leukemia cells [24], and is essential in resuming metabolic activity of quiescent B cells [21]. Enhanced TRPM7 expression and concomitant increases in Ca^{2+} influx have been linked to fibroblast proliferation, differentiation and fibrogenesis in human atrial fibrillation [25]. Thymopoiesis is blocked with induction of TRPM7-deficiency at the onset of thymic T cell development in mice [26], and recent data indicate that TPRM7 channel activity might be needed for Fas-induced T cell apoptosis [9]. Other studies implicate TRPM7 in cell growth that is linked to cancer [27]. A variety of human carcinoma cells including gastric adenocarcinoma, breast cancer, and human head and neck carcinoma cells express TRPM7 in abundance [19, 20, 23]. Suppression of TRPM7 genetically or pharmaceutically has been shown to inhibit the growth of these cell types. Pharmacological inhibition of TRPM7 by waixenicin A, a highly potent and specific TRPM7 antagonist, arrests Jurkat T cells at the G0/G1 and G2/M phase [28]. Interestingly, TRPM7's role in differentiated, non-proliferating tissue seems to be at variance from that seen in proliferative cell types, as suppression of TRPM7 protects hippocampal neurons from reperfusion injury and neuronal death in ischemia [29].

Non-metallic halogens such as chlorine, iodine and bromine are salt-forming elements. Molecular iodine is an essential co-factor of thyroid hormones [30], possibly entering cells

by facilitated diffusion [31]. The sodium-iodide symporter (NIS) SLC5A5 transports the halide form of iodine, iodide (I^-), across the plasma membrane of thyroidal, salivary, gastric and lactating mammary tissues for further processing [32–34]. While iodine seems to reduce the burden of breast cancer growth in humans and animals, the role of iodide is less pronounced [35]. It is thought that this is due to a lack of functional NIS activity in the affected tissue: While 80 % of breast cancer specimen express NIS [36], only a fraction of iodide transport seems functional, as iodide concentrations in breast cancer tissue is lower than in normal breast tissue [36]. In vitro studies show that nonradioactive iodide can induce cell cycle arrest and cell death in systems with unregulated sodium-iodide transporter expression in thyroid-, lung-, and mammary-related cancer [37–40], although the underlying molecular mechanisms of iodide effects remain less clear.

Chloride is an essential anion critical to the proper function of many cellular processes including membrane voltage stabilization, maintenance of intracellular pH and organellar acidification, and cellular volume regulation [41]. Consequently, perturbation in chloride homeostasis leads to several human diseases [42]. Volume regulation participates in an array of physiological cell functions, such as epithelial secretion, migration, cell cycle progression and apoptosis [43]. Ion exchange represents the most efficient way by which cells can rapidly adjust their intracellular osmolarity to induce or counteract changes in cell volume. Typically, the loss or gain of ion osmolytes such as potassium, sodium and chloride is followed by the respective movement of water and adjustment of cell volume. We have previously shown that TRPM7 is modulated by osmotic gradients and causes osmolarity-induced changes in intracellular Ca^{2+} concentration [44], possibly mediating cell detachment or adherence following cell volume changes. We hypothesized that the inhibition or facilitation of TRPM7 by the relative osmotic pressure is due to molecular crowding by concentrating or diluting inhibitory effectors such as Mg^{2+} or Mg·nucleotides and a further, unidentified factor [44]. We here ask the question whether chloride and related halides could act as negative feedback inhibitors of TRPM7. We find that TRPM7 activity is synergistically regulated by cytosolic halides and Mg^{2+} and consequently could affect processes involving volume changes during necrosis and apoptosis in addition to regulating the availability of Mg^{2+} during cell proliferation.

Results

Regulation of TRPM7 by chloride ions

We have previously shown that mammalian TRPM7 is regulated by osmotic changes in the cellular environment [44], which often are accompanied by an activation of chloride conductances [41]. While regulation of TRPM7 activity is most likely linked to molecular crowding of the channel's most prominent inhibitors Mg^{2+} and Mg-nucleotides, a third, unidentified factor that is not removed by the cellular perfusion process during whole-cell patch clamp seemed to be involved. To determine whether changes in cellular chloride conditions might have an impact on TRPM7 activity we measured human TRPM7 (TRPM7) currents expressed in HEK293 cells after tetracycline (2.25 μM) incubation for 16–24 h using the whole-cell patch clamp technique as previously described [3]. We studied the current behavior of TRPM7 in the absence (Fig. 1a) or presence (Fig. 1a–f) of intracellular free Mg^{2+} (800 μM) and with varying the availability of intracellular and extracellular chloride in the solutions (high intra- and extracellular chloride concentrations (Fig. 1a, b open squares), high intracellular chloride with low extracellular chloride (Cl^-) solution (Fig. 1a, b filled squares), low Cl^- both intracellularly and extracellularly (Fig. 1a, b filled circles) and standard solutions (see "Methods", Fig. 1a, b open circles). We previously have shown that removal of extracellular sodium by replacing NaCl with 140 mM NMDG-Cl had no effect on TRPM7 currents [3]. Currents sizes were assessed at −80 mV and +80 mV, averaged and plotted over the time of the experiment. Only outward TRPM7 currents at +80

mV are depicted in Fig. 1 for clarity purposes. Inward currents of TRPM7 behaved in analogy to their outward counterparts (data not shown and Fig. 3).

Interestingly, when retaining the Mg^{2+} concentration in the patch solution at physiological intracellular levels of 800 μM, high intracellular chloride strongly suppressed TRPM7 currents (Fig. 1b, open and filled squares), indicating a synergistic effect of Mg^{2+} and Cl^- on TRPM7 channels. Removal of extracellular chloride resulted in overall larger TRPM7 current sizes (Fig. 1a–d), however did not significantly alter the inhibitory capacity of intracellular chloride in combination with 800 μM intracellular Mg^{2+} ($[Mg^{2+}]_i$) (Fig. 1c–e): Dose–response curve fits resulted in similar IC_{50} values for low external chloride conditions (IC_{50} = 82 ± 6 mM) and high chloride conditions (IC_{50} = 99 ± 9 mM). The synergistic effect of Mg^{2+} and chloride could also be observed in native human TRPM7-like currents as assessed in HEK293 fibroblasts (Supp. Fig. 1). Taken together, these data show that intracellular chloride-induced TRPM7 inhibition requires $[Mg^{2+}]_i$ as an obligatory co-factor.

Regulation of TRPM7 by halides

We next investigated whether halides such as bromide or iodide could also cause inhibition of TRPM7 activity. Whole-cell patch clamp experiments were performed in extracellular solutions containing regular chloride concentrations (154 mM). Intracellular bromide affected TRPM7 currents in a similar fashion as chloride in that inhibition of currents required the presence of $[Mg^{2+}]_i$ (Fig. 2b, e and g). Interestingly, internal iodide suppressed TRPM7 currents largely independent of $[Mg^{2+}]_i$ (Fig. 2c, f and h), although the presence of Mg^{2+} shifted the IC_{50} of iodide-mediated inhibition twofold to the left, from an IC_{50} of 120 ± 6 mM without Mg^{2+} (Fig. 2i, open circles) to an IC_{50} of 59 ± 1 mM with 800 μM Mg^{2+} (Fig. 2i, filled circles). These data demonstrate that different halides inhibit TRPM7 in the presence of intracellular Mg^{2+}, but iodide can do so independently of this divalent ion.

Halide-induced inhibition of TRPM7 is facilitated by Mg·ATP

TRPM7 activity is regulated by a variety of physiological and patho-physiological conditions, including inhibition by Mg·ATP [3, 5], voltage-dependent Mg^{2+} block [3, 6], acidic pH [10, 11] and current facilitation by cAMP [15]. We investigated involvement of cAMP in chloride-induced inhibition of TRPM7 by perfusing cells with intracellular solution supplemented with 100 μM cAMP in addition to high chloride concentration (154 mM) and 800 μM Mg^{2+}. This did not reverse the suppression of the current (data not shown). Variation of Cl^- concentrations in intracellular or extracellular solutions has been reported change Cl^- transport across the cell membrane [45, 46]. However, none of the tested Cl^- channel blockers glibenclamide (100 μM) DIDS (100 μM) or tamoxifen (100 μM), nor the Na–K–Cl co-transporter inhibitor bumetanide (100 μM) were effective in reducing chloride-induced inhibition of TRPM7 (data not shown). Thus, inhibition of TRPM7 by intracellular Cl^- seems independent of cAMP or Cl^- transport mechanisms.

We next investigated whether intracellular Mg·ATP could enhance halide-mediated inhibition of TRPM7 whilst keeping $[Mg^{2+}]_i$ constant at 800 μM. We constructed dose–response curves to increasing halide concentrations at different fixed Mg·ATP concentrations (0, 1, 2, 4 and 6 mM). IC_{50} values for chloride varied between 112 ± 8 mM for 0 Mg·AT P to 69 ± 3 mM in the presence of 6 mM Mg·ATP (Fig. 3a). IC_{50} values for bromide varied between 88 ± 6 mM for 0 Mg·AT P to 35 ± 1 mM in the presence of 6 mM Mg·ATP (Fig. 3b). IC_{50} values for iodide varied between 57 ± 2 mM for 0 Mg·AT P to 32 ± 2 mM in the presence of 6 mM Mg·ATP (Fig. 3c). These data reveal a similar additive inhibitory effect of Mg·ATP across the three halides investigated, amounting to about twofold between extreme Mg·ATP concentrations (0 and 6 mM), and about 50 % increase in inhibitory efficacy when looking at more physiological Mg·ATP concentrations (2–4 mM).

This indicates that both Mg^{2+} and Mg·ATP can synergize with the halides in reducing TRPM7 channel activity.

Acidic pH, divalent-free conditions and chloride inhibition of TRPM7

We next investigated whether inhibition by halides could be removed through manipulating the channel permeation pathway. Here, we focused on chloride and exposed cells to acidic pH, which under regular conditions causes greatly enhanced inward currents due to a change in channel selectivity that allows Na^+ ions to pass through TRPM7 [11]. TPRM7 currents were allowed to fully activate over 200 s, at which time cells were superfused with an experimental solution similar in composition as the bath solution except that the pH was adjusted to 4.0. Since only inward currents were affected by acidification, we only depict the analysis of currents measured at −80 mV (Fig. 3). During acidification with pH 4.0, the TRPM7 current response was similar in high (Fig. 3d, filled circles) or low (Fig. 3d, open circles) internal chloride conditions in that both had greatly enhanced inward currents carried by TRPM7. A similar enhancement of TRPM7 currents was observed in the presence of regular intracellular chloride (14 mM) and 800 μM Mg^{2+} (Fig. 3e, open circles). Interestingly, however, acidification was unable to counteract the block of TRPM7 induced by the combination of high chloride and its co-factor Mg^{2+} (Fig. 3e, h, closed circles).

In a second set of experiments we investigated divalentfree (DVF) conditions, which also enables TRPM7 to conduct Na^+ ions. Currents were allowed to fully activate over 200 s, at which time cells were superfused with a solution similar in composition as the bath solution except for the nominal absence of divalent cations. Without intracellular Mg^{2+}, superfusing cells with DVF solution made no difference in the current response regardless whether intracellular chloride was high (154 mM, Fig. 3f, closed circles) or low (14 mM, Fig. 3f). Removal of external divalents enhanced TRPM7 currents also when internal chloride was kept low and 800 μM Mg^{2+} was added to the solution (Fig. 3g, open circles). In analogy to the observations with acidic pH, however, the combined presence of high intracellular chloride (154 mM) and 800 μM $[Mg^{2+}]_i$ inhibited TRPM7 even under DVF conditions (Fig. 3g, i). These data further confirm that chloride and Mg^{2+} synergistically inhibit TRPM7 and this inhibition remains effective when the channel permeation pathway is experimentally rendered non-selective.

Role of the TRPM7 kinase domain

We previously reported that mutating TRPM7's kinase domain changes the Mg^{2+} sensitivity of the channel, with point mutants targeting phosphorylation activity (K1648R and G1799D) decreasing the inhibition by $[Mg^{2+}]_i$ and complete removal of the kinase domain (TRPM7 Δ-kinase) strongly increasing sensitivity to this divalent ion [7]. The current understanding is that TRPM7 possesses two dominant Mg^{2+} binding sites, one on the kinase domain and the other on the channel proper. The latter has a strong binding affinity to Mg2+ and removal of the kinase domain exposes this site [7]. The binding site on the kinase domain coordinates the sensitivity of TRPM7 to various Mg·nucleotides, whereas the binding site on the channel does not discriminate and mainly recognizes Mg^{2+} binding [5]. Since chloride-mediated inhibition of TRPM7 critically depends on the presence of $[Mg^{2+}]_i$, we wondered whether those binding sites might be involved. For this set of experiments we focused on the two physiologically active halides, chloride and iodide. Whole-cell patch clamp experiments were performed in analogy to Fig. 1 for cells overexpressing either the K1648R or G1799R mutant of TRPM7 in tetracycline-induced HEK293 cells [7]. Both mutants behaved similarly to wild-type TRPM7 channels, in that chloride inhibited currents only in the presence of physiological intracellular Mg^{2+} (Fig. 4b). In contrast, removing the complete kinase domain made chloride inhibition of TRPM7 independent of Mg^{2+} (Fig. 4a, b). Furthermore, when testing intracellular iodide, the TRPM7 Δ-kinase was even more

sensitive to inhibition compared to wild-type TRPM7, shifting the IC_{50} of iodide from ~60 mM to an IC_{50} of 31 ± 3 mM (Figs. 2e, 4c, d). Thus it seems that the putative high-affinity Mg^{2+} binding site within the channel domain is involved in the coordination of halide binding and inhibition of the TRPM7 conductance pathway.

Regulation of TRPM6 by halides

The TRPM6 channel has the highest sequence similarity to TRPM7 (52 % identical, [16, 17]) and is also regulated by intracellular Mg^{2+} [47]. We investigated whether halides would interfere with TRPM6 activity in a similar manner as TPRM7, and assessed the two physiologically relevant ions chloride and iodide. We transiently overexpressed human TRPM6 in HEK293 cells and performed whole-cell patch clamp experiments perfusing TRPM6-expressing HEK93 cells with high (154 mM) or low (14 mM) concentrations of chloride in the absence of intracellular Mg^{2+} and normal extracellular solutions. Fig. 4 illustrates that chloride alone did not interfere with TRPM6 channel activity or shape of the current–voltage behavior (Fig. 4e, f). As expected, increasing $[Mg^{2+}]_i$ suppressed TRPM6 currents (Fig. 4e, open triangles), however, chloride did not add to this inhibition in a statistically significant manner, even at physiological Mg^{2+} levels of 800 μM (Fig. 4e, filled triangles). The normalized dose–response behavior to chloride and $[Mg^{2+}]_i$ is depicted in Fig. 4g. We should note that while we used the same TRPM6 vector as published [47, 48], our experiments yield a much higher sensitivity to intracellular Mg^{2+}. We currently do not have an explanation for this discrepancy. While chloride interferes little with TRPM6 activity, iodide does so, albeit only at high concentrations (154 mM, Fig. 4h filled circles) and in synergy with increased $[Mg^{2+}]_i$. As the normalized dose–response data indicate, 100 μM intracellular Mg^{2+} suppresses TRPM6 currents in the absence of iodide (and regular 14 mM internal chloride conditions) by 60 % (Fig. 4h, open circles). Replacing chloride with 14 mM intracellular iodide causes a small current reduction in the absence of Mg^{2+} and TRPM6 current inhibition by an additional 70 % compared to control (0 Mg^{2+}) (Fig. 4h open squares). Adding 154 mM iodide intracellularly suppresses TRPM6 current by 52 % in the absence of any Mg^{2+}, and adding 100 μM Mg^{2+} produces an almost 100 % inhibition of currents (93 %, Fig. 4h filled circles). These data indicate that TRPM6 and TRPM7 are differentially regulated by halides in that TRPM6 is not sensitive to chloride and only marginally affected by intracellular iodide.

TRPM7 and iodide in breast cancer cell proliferation

It has been shown that cancer cell growth of human MCF-7 cells depends on TRPM7 expression [20]. These cells have low expression levels of the iodide transporter SLC5A5, whose expression levels can be enhanced by all-trans retinoic acid (tRA) leading to cellular accumulation of iodide [49]. We therefore used this model to correlate endogenous TRPM7-like current activity, inhibition by halides, and cell growth. We previously coined native TRPM7-like currents as magnesium-nucleotide metal current MagNuM [3]. Similarly to heterologously expressed TRPM7, MagNuM currents in MCF-7 cells were inhibited by high intracellular chloride only in the presence of intracellular Mg^{2+} (800 μM; Fig. 5a, b, e left panel). However, iodide strongly suppressed MagNuM even in the absence of intracellular Mg^{2+} (Fig. 5c, e right panel) so that simply adding I^- to the standard pipette solution completely abolished the development of any MagNuM currents (Fig. 5d).

We next assessed cell growth in the absence and presence of 1 mM sodium iodide (NaI) in the culture medium, but observed no inhibitory effect compared to control cells, presumably because of low levels of I^- transport capacity in these cells (Fig. 5i open and right-tilted striped bars, respectively). To increase SLC5A5 expression and I^- transport capacity, we exposed MCF-7 cells to all-trans retinoic acid (tRA) and confirmed that incubation with 1 μM tRA for 72 h strongly increases SLC5A5 mRNA expression levels in these cells (Fig.

5f). We also confirmed that addition of external iodide (1 mM) did not significantly interfere with SLC5A5 expression levels, either in the presence or absence of tRA (Fig. 5f). We repeated tRA exposure with or without external iodide and confirmed that both TRPM7 (Fig. 5g) and TRPM6 expression levels (Fig. 5h) remained unaltered by any of these treatments. Finally, we asked whether the increased iodide uptake due to increased SLC5A5 expression would affect cell proliferation. tRA itself is known to inhibit cell growth unrelated to enhanced I^- transport via SLC5A5 [49]. Indeed, treating MCF-7 cells with tRA significantly reduced cell growth (Fig. 5i left-tilted striped bars) compared to untreated controls (Fig. 5i open bars). However, MCF-7 cells treated with both tRA and 1 mM external iodide significantly reduced cell proliferation at day 3 ($P < 0.01$) and later above and beyond the inhibition exerted by tRA alone (Fig. 5i cross-hashed bars; $P < 0.01$).

Discussion

TRPM7 is a ubiquitously expressed divalent cation channel critically involved in embryo development [4, 26], cell proliferation [3, 21], and systemic Mg^{2+} homeostasis [4]. Pathophysiologically, TRPM7 has been implicated in reperfusion injury after global ischemia [29] and cancer [27]. Changes in cell volume regulate TRPM7 activity through changes in the cytosolic concentrations of free Mg^{2+}, Mgnucleotides and a further unrecognized factor [44]. We here identify chloride ions as a novel regulatory mechanism suppressing TRPM7 channel activity in synergy with intracellular free Mg^{2+}. Specifically, we find that all halide ions investigated (chloride, bromide, iodide) inhibit TRPM7 in synergy with intracellular Mg^{2+}, and this is facilitated by the Mg·ATP binding site in the channel's kinase domain. Intracellular Mg·ATP further strengthens this inhibition, and neither acidic conditions nor removal of divalent ions can eliminate the synergistic block. Only iodide, however, suppresses TRPM7 independently of Mg^{2+}, presumably by directly binding to the proposed Mg^{2+} binding site within the channel domain. Halide-induced block can also be observed when measuring endogenous TRPM7-like currents in MCF-7 human breast cancer cells, and upregulation of the sodium-iodide symporter in these cells leads to arrest of cell proliferation when exposed to increased external iodide concentrations.

Chloride regulation of TRPM7 is dependent on intracellular magnesium

Chloride is the most abundant negatively charged ion in mammals, with extracellular concentrations at about 100 mM. Intracellular chloride concentrations can vary between ~5 and 41 mM, depending on the respective chloride transport mechanism in the plasma membrane [50–52]. In developing neurons, oxygen-glucose deprivation causes prolonged intracellular chloride accumulation to up to 54 mM [53]. Intracellular chloride storage compartments are reported to accumulate chloride up to 110 mM [54]. Thus cells have at least two storage compartments available to controllably access this critical anion. The physiological role of chloride transporters is well understood, however, little is know about chloride-induced regulatory effects on specific ion channel mechanisms. Our data show that high extracellular chloride conditions dampen TRPM7 activity (Fig. 1), although this effect bears little influence on the regulation of TRPM7 by intracellular chloride (Fig. 1e). Extracellular chloride has been reported to regulate the epithelial sodium channel ENaC [55]. On ASIC-1a, which stands for acidsensing ion channel 1a, three amino acid residues have been identified through which chloride modulates desensitization kinetics of the channel [56]. Whether TRPM7 activity is regulated directly by chloride binding to the outer mouth of the channel or by an independent mechanism remains to be determined. Interestingly, several studies reported increased TRPM7-like current activity immediately upon whole-cell establishment where loss of cytosolic Mg^{2+} and Mg·AT P can be assumed minimal. This might be explained by the use of low extracellular chloride conditions in these

studies leading to a loss of intracellular chloride and thus overall higher TRPM7 channel activity [6, 57–60].

Our data further show that TRPM7 currents are insensitive to increased intracellular chloride concentrations unless accompanied by intracellular Mg^{2+}. Previous work established an IC_{50} of TRPM7 to $[Mg^{2+}]_i$ in low intracellular chloride conditions of around 800 μM [5]. When increasing chloride to 154 mM inside the cell and using 800 μM Mg^{2+}, currents were suppressed by around 90 % compared to normal chloride (Fig. 1e, f). This shows that $[Mg^{2+}]_i$ is a critical co-factor of chloride-induced feedback inhibition on TRPM7 currents and the relative individual concentration changes of these two molecules synergistically regulate overall TRPM7 activity. This synergy is further enhanced in the presence of Mg·ATP (Fig. 3). Interestingly, TRPM6, the ion channel with the highest sequence homology to TRPM7, does not respond to chloride regulation (Fig. 4). Other ion channels and cellular mechanisms are influenced by increased intracellular chloride, which include the sodium epithelial channel ENaC [61, 62], thereby reducing sodium influx in taste cells [63]. In hippocampal granule neurons, synaptic transmission mediated by GABA receptors is dampened by intracellular chloride accumulation due to membrane depolarization [64, 65]. Our previous work showed that changes in osmotic pressure cause TPRM7-mediated changes in intracellular Ca^{2+} levels most likely by changes in molecular crowding of solutes interfering with TRPM7 activity, as hypo-osmotic conditions caused TRPM7 activation only in the presence of intracellular Mg^{2+} or Mg·AT P [44]. In contrast, inhibition of the current by hyperosmolarity proceeded largely independent of those two regulators, which led us to postulate a mechanism or factor that resists washout imposed by cell perfusion. Since chloride conditions were kept constant for these experiments, this anion may represent part of this additional regulatory mechanism.

At least 50 % of cell death underlying reperfusion injury after cerebral infarct is thought to be due to compromised cell volume regulation leading to cell swelling with subsequent bursting [66]. This is partially mediated by Ca^{2+} influx through TRPM7, as decreased extracellular Ca^{2+} and Mg^{2+} during reperfusion, loss of intracellular ATP and changes in tissue hydrogen balance influence TRPM7 channel activity and selectivity [3, 10, 11]. Interestingly, neither strong extracellular acidification nor removal of divalent ions from the extracellular milieu was able to counteract the synergistic block of TRPM7 by chloride and Mg^{2+} (Fig. 3). Two models are plausible, one where chloride either induces a conformational change of TRPM7 to an inactivated state, or causes a permanent Mg^{2+} block of the TRPM7 pore. Such suppression of TRPM7 activity under cellular stress accompanied by loss of ion movement regulation and concomitant change in chloride balance might prove supportive in temporarily protecting cell function.

The Mg·ATP binding site of the TRPM7 kinase domain coordinates channel inhibition by chloride

Previous work has shown that TRPM7 contains at least two binding sites that coordinate Mg^{2+} binding. One site is located on the protein's kinase domain and coincides with amino acid residues participating in nucleotide binding (K1648) and phosphor-transfer (G1799) [7]. The K1648 binding site can discriminate between the type of Mg·nucleotide binding to TRPM7, preferring AT P and GTP over CTP and ITP [5]. The second Mg^{2+} binding site is located on the channel domain, as removal of the complete kinase after residue 1569 renders the protein highly sensitive to intracellular Mg^{2+}. Interestingly, removal of the kinase domain after residue position 1599 produces a non-functional channel [8] whereas truncating the kinase at an earlier amino acid (aa 1510) fully recovers TRPM7 channel activity [9]. It is tempting to speculate that the region between amino acids 1510 and 1599 supports proper coordination with the second Mg^{2+} binding site. Two separate binding sites on TRPM7 with differing affinities to Mg^{2+} binding have further been described in great

detail in a cell free system [6, 60]. We here investigated the chloride sensitivity of three kinase mutants, two with a single point mutation relevant to Mg-nucleotide coordination (K1648R, G1799D) and the complete kinase deletion after residue 1569 [7]. Our findings indicate that the Mg·ATP binding site (K1648), but not the phospho-transfer site (G1799), is involved in coordinating chloride inhibition, since the latter remains sensitive to increased chloride, whereas the K1648R mutant is much less so (Fig. 4b). The binding site for chloride however seems to reside in the channel domain, since even in the absence of the kinase domain the channel remains sensitive to chloride inhibition and furthermore becomes independent of $[Mg^{2+}]_i$ (Fig. 4a, b). This indicates that in the absence of the kinase domain, chloride can affect the channel without coordination through Mg^{2+}. It also confirms our previous observation that part of the osmosensitivity of TRPM7 resides in the channel domain, since TRPM7 delta kinase mutant is sensitive to osmotic pressure changes independently of the presence of Mg^{2+} [44].

TRPM7 inhibition by halides other than chloride

Typically, ion channels and transporters selective for chloride do not discriminate between halide species. In analogy, both bromide and iodide were able to inhibit TRPM7 in addition to chloride. Bromide, whose physiological role is less known, behaved similarly to chloride in that it required Mg^{2+} as co-factor to induce current inhibition (Fig. 2). Iodide, however, blocked TRPM7 not only twice as efficiently (Fig. 3; $IC_{50\ chloride}$ = 67 mM compared to $IC_{50\ iodide}$ = 32 mM (at 800 μM Mg^{2+} and 4 mM Mg·ATP)), but could also interfere with channel activity in the absence of any Mg^{2+} or Mg·ATP, albeit much less potently (Fig. 2; $IC_{50\ iodide\ 0\ Mg}$ = 120 mM). Removal of the TPRM7 kinase domain showed that iodide seems able to bind directly and effectively to the protein's channel domain, even without co-factors such as Mg^{2+} and Mg-nucleotides (Fig. 4). Thus, block of TRPM7 by synergistic interaction between Mg^{2+} and halides seems coordinated through the Mg·ATP binding site involving amino acid residue 1648 in the kinase domain, with iodide having the ability to shunt this process. This does not seem to involve the phospho-transfer activity of the kinase, as the catalytically inactive G1799D mutant retains its chloride sensitivity. Interestingly, another serine/threonine kinase, with-no-lysine kinase 3 (WNK3), seems to be a chloride-sensing enzyme activated by reductions of intracellular chloride levels and regulating potassium- and sodium-coupled chloride transporters [67].

Regulation of other ion channels by chloride

Alterations in cell volume are key events in necrosis, apoptosis and cell proliferation. They necessitate changes in cytosolic potassium and chloride accompanied by mandatory water movement [41]. Since the Na^+/K^+ AT Pase rapidly counteracts any changes in potassium concentrations, the net result is the move of chloride ions across the plasma membrane thereby affecting intracellular chloride concentrations. While the movement of sodium and potassium is well studied during volume changes, much less is known of chloride. Cytosolic chloride changes underlie the osmoregulation of ENaC gene expression [68], the regulation of cell proliferation through stress-activated protein kinases [69] and the regulation of the intrinsic apoptotic pathway in Jurkat T cells [70]. Repression of chloride ion channels and the movement of sodium and chloride in multi-drug resistant Ehrlich ascites tumor cells impair apoptotic volume decrease (AVD) and allow escape from cell death [71]. Slow and regulated volume increases during cell proliferation prepare for cell division and the role of TRPM7 to provide the necessary amount of cytosolic Mg^{2+} for appropriate conclusion of cell growth is well documented [72]. However, Mg^{2+} gradients across the plasma membrane are two-fold at best compared to Ca^{2+}, which has a 10,000-fold difference in driving force. With fast cell volume changes TRPM7's ability to conduct Ca^{2+} may be prevalent in supporting regulatory volume adjustments, whereby hyperosmotic suppression of TRPM7

leads to a reduction of intracellular Ca^{2+} as opposed to a possible increase during hypo-osmotic conditions.

Iodide, TRPM7, and cell proliferation

Iodine deficiency is a known risk factor for thyroid and breast cancer [30, 73]. Both are tissues that concentrate iodine via the sodium-iodide symporter (NIS). Thyroid cells can accumulate up to 60 times the extracellular iodide when using 300 μM in the bath milieu implying intracellular iodide levels of up to 18 mM [74], while another study reported 2 mM iodide concentrations achieved by overexpression of pendrin, an iodide-specific apical porter [75]. Iodine consumption is thought to be protective for breast cancer in humans based on its anti-oxidative properties, while the role of iodide is less clear. Suppression of TRPM7 either genetically [21] or pharmaceutically [28] induces arrest of cancer cell proliferation. Here, we show that elevated external iodide (1 mM) suppresses human breast cancer MCF-7 cell proliferation only when upregulating NIS expression by retinoic acid (Fig. 5i). While further exploration is needed, it is tempting to speculate that this might be contributing to a negative feedback inhibition of TRPM7 channels exposed to higher iodide concentrations in the vicinity of active iodide transport by NIS. Future investigations should clarify whether TRPM7 represents a possible molecular mechanism underlying the anti-proliferative characteristics of intracellular iodide accumulation.

Materials and methods

Cell culture and transfection

HEK293 wild-type cells and HEK293 cells stably expressing tetracycline-inducible human TRPM7 protein, TRPM7 mutants K1648R, G1788D and kinase-truncated TRPM7 mutation (TRPM7 Δ-kinase, [7]), were cultured in DME medium supplemented with 10 % fetal bovine serum, blasticidin (5 μg ml^{-1}) and zeocin (0.4 mg ml^{-1}) in a 5 % CO_2-humidified atmosphere at 37 °C. Protein expression was induced the day preceding the experiments by adding 1 μg ml^{-1} tetracycline to the culture medium. Patch-clamp measurements were performed 16–24 h post-induction. For human TRPM6 experiments, HEK293 wild-type cells were transiently transfected with pCINeo-IRES-GFP-hTRPM6 constructs using Lipofectamine 2000 (Invitrogen). Whole-cell patch clamp experiments were carried out 30 h post-transfection. Expression of TRPM6 constructs was identified by green fluorescence. MCF-7 cells were grown in Eagle's minimum essential medium containing 10 % fetal bovine serum and penicillin (50 IU/ml)-streptomycin (50 μg ml^{-1}) at 37 °C in a humidified atmosphere of 5 % CO_2 in air.

Solutions

For patch-clamp experiment, cells were kept in the bath solution containing (in mM): 150 NaCl, 1 $CaCl_2$, 1 $MgCl_2$, 10 HEPES and 10 glucose for the solution of high external Cl^- concentration (high $[Cl^-]_o$); pH 7.2, with osmolarity typically ranging from 295 to 325 mOsm. HEPES was replaced by MES for solutions at pH ≤ 6.0. Solutions of low external Cl^- concentration (low $[Cl^-]_o$), NaCl was equimolarly substituted by Na-gluconate (see also Table 1). In divalent-free solution (DVF), divalent ions were removed and 0.5 mM EDTA was added. Pipette solution contained (in mM): 150 CsCl, 10 HEPES for the solution of high intracellular Cl^- concentration (high $[Cl^-]_i$), and 140 Cs-glutamate, 10 CsCl, 10 HEPES for the solution of low intracellular Cl^- concentration (low $[Cl^-]_i$); pH 7.2 was adjusted with CsOH. The concentration of intracellular Mg^{2+} ($[Mg^{2+}]_i$) was clamped at 0 or 0.8 mM as calculated with WebMaxC (http://www.stanford.edu/~cpatton/webmaxcS.htm, see Table 2). Table 3 lists the internal chloride concentrations and solution compositions for dose–response curves. For bromide and iodide experiments, the internal pipette solution contained (in mM): 6.4 CsCl, 13.6, 48.6, 83.6, 118.6, or 153.6 CsBr or CsI, 1 EDTA , 1

EGTA 1.8 $MgCl_2$, 10 HEPES. The pH was adjusted to 7.2 and osmolarity was between 290 and 310 mOsm. Liquid junction potentials for the different halide internal and external solutions are given in Table 4. We measured the liquid junction potential induced by external and internal chloride changes taking advantage of the linear current–voltage (I/V) relationship of TRPM2 currents, which reverse at 0 mV [76]. Any change in chloride concentration will induce a shift in the apparent reversal potential of the current away from 0 mV, reflecting the actual liquid junction potential imposed by the composition of the solution. We recorded TRPM2 whole cell currents in HEK293 cells overexpressing the protein activated with 1 mM ADPR in the pipette solution [76] and assessed the liquid junction potentials under various chloride conditions (Table 4).

Patch-clamp experiments

Patch-clamp experiments were performed in the tight-seal whole-cell configuration at 21–25 °C. High-resolution current recordings were acquired by a computer-based patch-clamp amplifier system (EPC-9, HEKA). Patch pipettes had resistances between 2 and 4 MΩ after filling with the standard pipette solution. Immediately following establishment of the whole-cell configuration, voltage ramps of 50 ms duration spanning the voltage range of −100 to +100 mV were delivered from a holding potential of 0 mV at a rate of 0.5 Hz. All voltages were corrected for liquid junction potential (see Table 4) to account for changes in halide concentration. Currents were filtered at 2.9 kHz and digitized at 500-μs intervals. Capacitive currents and series resistance were determined and corrected before each voltage ramp using the automatic capacitance compensation of the EPC-9. In HEK293 cells overexpressing TRPM7, data were analyzed without correcting for initial currents, since there was a significant level of basal TRPM7 conductance at the time of whole-cell establishment (break-in). The low-resolution temporal development of currents at a given potential was extracted from individual ramp current records by measuring the current amplitudes at voltages of −80 mV and +80 mV, respectively.

RNA isolation, cDNA synthesis and quantitative real time PCR

Quantitative real time PCR (qPCR) was employed to examine the mRNA expression levels of SLC5A5, TRPM6 and TRPM7 using β-actin (ACTB) as a reference for normalization. MCF-7 cells were harvested from culture with the pretreatment of PBS vehicle, 1 mM NaI, 1 μM tRA (Sigma) or the combination of 1 mM NaI and 1 μM tRA for 72 h. Total RNA was extracted using the RNeasy Mini kit (Qiagen, Valencia, CA). The random priming was utilized to convert mRNA to cDNA by ABI's High Capacity cDNA RT Kit with RNase Inhibitor (Applied Biosystems, Life Technologies, Foster City, CA). The qPCR was performed using the ABIs' HT7900 FAST Real-Time PCR System (Applied Biosystems, Life Technologies) and the ABI's POWER SYBRGreen (Applied Biosystems, Life Technologies) according to the manufacturers' protocols. Gene-specific primer pairs of human TRPM6, TRPM7, SLC5A5, and ACTB were purchased from Qiagen.

Cell count and viability

MCF-7 cells were grown in 12-plate at a density of 1.5×10^5 cells ml^{-1} $well^{-1}$. The cells were treated with PBS vehicle, 1 mM NaI, 1 μM tRA and the mixture of 1 mM NaI and 1 μM tRA. MCF-7 cell growth was assessed with the standard Malassez cell method at each of the indicated time (2d–4d). Briefly, cells were isolated to single status by trypsinization and stained by Trypan blue. Cell counts were performed four times. The result of each time point shown in the growth histogram (Fig. 5i) represents averages from quadruplicate cultures.

Data analysis

Data were analyzed with FitMaster (HEKA) and IgorPro (WaveMetrics). Where applicable, statistical errors of averaged data are given as means ± SEM with n determinations and statistical significance was assessed by Student's t test. Currents (in Ampere) were normalized to cell size (capacitance in Farad) assessed immediately upon break-in. Dose–response curves were calculated using the function $f(x) = (Y_{max} \times (1/(1 + (IC_{50}/x)^n)))$, where Y_{max} is the maximal normalized current, IC_{50} is the concentration at which inhibition is half maximal, x is the concentration, and n is the Hill coefficient.

Supplementary Material

Refer to Web version on PubMed Central for supplementary material.

Acknowledgments

Expert technical expertise provided by Stephanie Johne and Christopher Maggio. Thank you to Dr. René J.M. Bindels and Dr. Alexey Ryazanov for kindly providing pCINeo-IRES-GFP-hTRPM6 construct. This work was supported by the National Institute for General Medical Science at the National Institutes of Health [P01GM078195 to A.F.].

References

1. Ryazanova LV, Dorovkov MV, Ansari A, Ryazanov AG. Characterization of the protein kinase activity of TRPM7/ChaK1, a protein kinase fused to the transient receptor potential ion channel. J Biol Chem. 2004; 279:3708–3716. [PubMed: 14594813]
2. Runnels LW, Yue L, Clapham DE. TRP-PLIK, a bifunctional protein with kinase and ion channel activities. Science. 2001; 291:1043–1047. [PubMed: 11161216]
3. Nadler MJ, Hermosura MC, Inabe K, Perraud AL, Zhu Q, Stokes AJ, Kurosaki T, Kinet JP, Penner R, Scharenberg AM, et al. LT RPC7 is a Mg.AT P-regulated divalent cation channel required for cell viability. Nature. 2001; 411:590–595. [PubMed: 11385574]
4. Ryazanova LV, Rondon LJ, Zierler S, Hu Z, Galli J, Yamaguchi TP, Mazur A, Fleig A, Ryazanov AG. TRPM7 is essential for Mg(2+) homeostasis in mammals. Nat Commun. 2010; 1:109. [PubMed: 21045827]
5. Demeuse P, Penner R, Fleig A. TRPM7 channel is regulated by magnesium nucleotides via its kinase domain. J Gen Physiol. 2006; 127:421–434. [PubMed: 16533898]
6. Chokshi R, Matsushita M, Kozak JA. Detailed examination of Mg2+ and pH sensitivity of human TRPM7 channels. Am J Physiol Cell Physiol. 2012; 302:C1004–C1011. [PubMed: 22301056]
7. Schmitz C, Perraud AL, Johnson CO, Inabe K, Smith MK, Penner R, Kurosaki T, Fleig A, Scharenberg AM. Regulation of vertebrate cellular Mg2+ homeostasis by TRPM7. Cell. 2003; 114:191–200. [PubMed: 12887921]
8. Matsushita M, Kozak JA, Shimizu Y, McLachlin DT, Yamaguchi H, Wei FY, Tomizawa K, Matsui H, Chait BT, Cahalan MD, et al. Channel function is dissociated from the intrinsic kinase activity and autophosphorylation of TRPM7/ChaK1. J Biol Chem. 2005; 280:20793–20803. [PubMed: 15781465]
9. Desai BN, Krapivinsky G, Navarro B, Krapivinsky L, Carter BC, Febvay S, Delling M, Penumaka A, Ramsey IS, Manasian Y, et al. Cleavage of TRPM7 releases the kinase domain from the ion channel and regulates its participation in Fas-induced apoptosis. Develop. Cell. 2012; 22:1149–1162.
10. Kerschbaum HH, Kozak JA, Cahalan MD. Polyvalent cations as permeant probes of MIC and TRPM7 pores. Biophys J. 2003; 84:2293–2305. [PubMed: 12668438]
11. Jiang J, Li M, Yue L. Potentiation of TRPM7 inward currents by protons. J Gen Physiol. 2005; 126:137–150. [PubMed: 16009728]

12. Wei WL, Sun HS, Olah ME, Sun X, Czerwinska E, Czerwinski W, Mori Y, Orser BA, Xiong ZG, Jackson MF, et al. TRPM7 channels in hippocampal neurons detect levels of extracellular divalent cations. Proc Natl Acad Sci USA. 2007; 104:16323–16328. [PubMed: 17913893]
13. Monteilh-Zoller MK, Hermosura MC, Nadler MJ, Scharenberg AM, Penner R, Fleig A. TRPM7 provides an ion channel mechanism for cellular entry of trace metal ions. J Gen Physiol. 2003; 121:49–60. [PubMed: 12508053]
14. Runnels LW, Yue L, Clapham DE. The TRPM7 channel is inactivated by PIP(2) hydrolysis. Nat Cell Biol. 2002; 4:329–336. [PubMed: 11941371]
15. Takezawa R, Schmitz C, Demeuse P, Scharenberg AM, Penner R, Fleig A. Receptor-mediated regulation of the TRPM7 channel through its endogenous protein kinase domain. Proc Natl Acad Sci USA. 2004; 101:6009–6014. [PubMed: 15069188]
16. Schlingmann KP, Weber S, Peters M, Niemann Nejsum L, Vitzthum H, Klingel K, Kratz M, Haddad E, Ristoff E, Dinour D, et al. Hypomagnesemia with secondary hypocalcemia is caused by mutations in TRPM6, a new member of the TRPM gene family. Nat. Gen. 2002; 31:166–170.
17. Walder RY, Landau D, Meyer P, Shalev H, Tsolia M, Borochowitz Z, Boettger MB, Beck GE, Englehardt RK, Carmi R, et al. Mutation of TRPM6 causes familial hypomagnesemia with secondary hypocalcemia. Nat Gen. 2002; 31:171–174.
18. Abed E, Moreau R. Importance of melastatin-like transient receptor potential 7 and magnesium in the stimulation of osteoblast proliferation and migration by platelet-derived growth factor. Am J Physiol Cell Physiol. 2009; 297:C360–C368. [PubMed: 19474290]
19. Jiang J, Li MH, Inoue K, Chu XP, Seeds J, Xiong ZG. Transient receptor potential melastatin 7-like current in human head and neck carcinoma cells: role in cell proliferation. Cancer Res. 2007; 67:10929–10938. [PubMed: 18006838]
20. Guilbert A, Gautier M, Dhennin-Duthille I, Haren N, Sevestre H, Ouadid-Ahidouch H. Evidence that TRPM7 is required for breast cancer cell proliferation. Am J Physiol Cell Physiol. 2009; 297:C493–C502. [PubMed: 19515901]
21. Sahni J, Tamura R, Sweet IR, Scharenberg AM. TRPM7 regulates quiescent/proliferative metabolic transitions in lymphocytes. Cell Cycle. 2010; 9:3565–3574. [PubMed: 20724843]
22. Wykes RC, Lee M, Duffy SM, Yang W, Seward EP, Bradding P. Functional transient receptor potential melastatin 7 channels are critical for human mast cell survival. J Immunol. 2007; 179:4045–4052. [PubMed: 17785843]
23. Kim BJ, Park EJ, Lee JH, Jeon JH, Kim SJ, So I. Suppression of transient receptor potential melastatin 7 channel induces cell death in gastric cancer. Cancer Sci. 2008; 99:2502–2509. [PubMed: 19032368]
24. Tani D, Monteilh-Zoller MK, Fleig A, Penner R. Cell cycledependent regulation of store-operated I(CRAC) and Mg2+-nucleotide-regulated MagNuM (TRPM7) currents. Cell Calcium. 2007; 41:249–260. [PubMed: 17064762]
25. Du J, Xie J, Zhang Z, Tsujikawa H, Fusco D, Silverman D, Liang B, Yue L. TRPM7-mediated Ca2+ signals confer fibrogenesis in human atrial fibrillation. Circ Res. 2010; 106:992–1003. [PubMed: 20075334]
26. Jin J, Desai BN, Navarro B, Donovan A, Andrews NC, Clapham DE. Deletion of Trpm7 disrupts embryonic development and thymopoiesis without altering Mg2+ homeostasis. Science. 2008; 322:756–760. [PubMed: 18974357]
27. Wolf FI, Trapani V. Magnesium and its transporters in cancer: a novel paradigm in tumour development. Clin Sci. 2012; 123:417–427. [PubMed: 22671428]
28. Zierler S, Yao G, Zhang Z, Kuo WC, Porzgen P, Penner R, Horgen FD, Fleig A. Waixenicin A inhibits cell proliferation through magnesium-dependent block of transient receptor potential melastatin 7 (TRPM7) channels. J Biol Chem. 2011; 286:39328–39335. [PubMed: 21926172]
29. Aarts M, Iihara K, Wei WL, Xiong ZG, Arundine M, Cerwinski W, MacDonald JF, Tymianski M. A key role for TRPM7 channels in anoxic neuronal death. Cell. 2003; 115:863–877. [PubMed: 14697204]
30. Patrick L. Iodine: deficiency and therapeutic considerations. Alt Med Rev. 2008; 13:116–127.
31. Arroyo-Helguera O, Anguiano B, Delgado G, Aceves C. Uptake and antiproliferative effect of molecular iodine in the MCF-7 breast cancer cell line. Endo Rel Cancer. 2006; 13:1147–1158.

32. Venturi S. Is there a role for iodine in breast diseases? Breast. 2001; 10:379–382. [PubMed: 14965610]
33. Spitzweg C, Morris JC. The sodium iodide symporter: its pathophysiological and therapeutic implications. Clin Endo. 2002; 57:559–574.
34. Spitzweg C, Morris JC. Sodium iodide symporter (NIS) and thyroid. Hormones. 2002; 1:22–34. [PubMed: 17018435]
35. Eskin BA. Dietary iodine and cancer risk. Lancet. 1976; 2:807–808. [PubMed: 61482]
36. Tazebay UH, Wapnir IL, Levy O, Dohan O, Zuckier LS, Zhao QH, Deng HF, Amenta PS, Fineberg S, Pestell RG, et al. The mammary gland iodide transporter is expressed during lactation and in breast cancer. Nat Med. 2000; 6:871–878. [PubMed: 10932223]
37. Smerdely P, Pitsiavas V, Boyages SC. Evidence that the inhibitory effects of iodide on thyroid cell proliferation are due to arrest of the cell cycle at G0G1 and G2M phases. Endocrinol. 1993; 133:2881–2888.
38. Vitale M, Di Matola T, D'Ascoli F, Salzano S, Bogazzi F, Fenzi G, Martino E, Rossi G. Iodide excess induces apoptosis in thyroid cells through a p53-independent mechanism involving oxidative stress. Endocrinol. 2000; 141:598–605.
39. Zhang L, Sharma S, Zhu LX, Kogai T, Hershman JM, Brent GA, Dubinett SM, Huang M. Nonradioactive iodide effectively induces apoptosis in genetically modified lung cancer cells. Cancer Res. 2003; 63:5065–5072. [PubMed: 12941836]
40. Stoddard FR, Brooks AD, Eskin BA, Johannes GJ. Iodine alters gene expression in the MCF7 breast cancer cell line: evidence for an anti-estrogen effect of iodine. Int J Med Sci. 2008; 5:189–196. [PubMed: 18645607]
41. Lang F, Busch GL, Volkl H. The diversity of volume regulatory mechanisms. Int J Exp Cell Physiol Biochem Pharm. 1998; 8:1–45.
42. Planells-Cases R, Jentsch TJ. Chloride channelopathies. Biochim Biophys Acta. 2009; 1792:173–189. [PubMed: 19708126]
43. Hoffmann EK, Pedersen SF. Cell volume homeostatic mechanisms: effectors and signalling pathways. Acta Physiol. 2011; 202:465–485.
44. Bessac BF, Fleig A. TRPM7 channel is sensitive to osmotic gradients in human kidney cells. J Physiol (Lond). 2007; 582:1073–1086. [PubMed: 17510191]
45. Schomberg SL, Bauer J, Kintner DB, Su G, Flemmer A, Forbush B, Sun D. Cross talk between the GABA(A) receptor and the Na-K-Cl cotransporter is mediated by intracellular Cl. J Neurophysiol. 2003; 89:159–167. [PubMed: 12522168]
46. Lytle C, McManus T. Coordinate modulation of Na-K-2Cl cotransport and K-Cl cotransport by cell volume and chloride. Am J Physiol Cell Physiol. 2002; 283:C1422–C1431. [PubMed: 12372803]
47. Voets T, Nilius B, Hoefs S, Van der Kemp AW, Droogmans G, Bindels RJ, Hoenderop JG. TRPM6 forms the Mg2+ influx channel involved in intestinal and renal Mg2+ absorption. J Biol Chem. 2004; 279:19–25. [PubMed: 14576148]
48. Thebault S, Cao G, Venselaar H, Xi Q, Bindels RJ, Hoenderop JG. Role of the alpha-kinase domain in transient receptor potential melastatin 6 channel and regulation by intracellular AT P. J Biol Chem. 2008; 283:19999–20007. [PubMed: 18490453]
49. Willhauck MJ, Sharif-Samani B, Senekowitsch-Schmidtke R, Wunderlich N, Goke B, Morris JC, Spitzweg C. Functional sodium iodide symporter expression in breast cancer xenografts in vivo after systemic treatment with retinoic acid and dexamethasone. Breast Cancer Res Treat. 2008; 109:263–272. [PubMed: 17636401]
50. Zhou J-G, Ren J-L, Qiu Q-Y, He H, Guan Y-Y. Regulation of intracellular Cl- concentration through volume-regulated ClC-3 chloride channels in A10 vascular smooth muscle cells. J Biol Chem. 2005; 280:7301–7308. [PubMed: 15596438]
51. Garcia MA, Meizel S. Determination of the steady-state intracellular chloride concentration in capacitated human spermatozoa. J Androl. 1999; 20:88–93. [PubMed: 10100478]
52. Akabas MH. Chloride channels. Encyclopedia of Life Sciences. 2001:1–7.

53. Kakazu Y, Akaike N, Komiyama S, Nabekura J. Regulation of intracellular chloride by cotransporters in developing lateral superior olive neurons. J Neurosci. 1999; 19:2843–2851. [PubMed: 10191302]
54. Arosio D, Ricci F, Marchetti L, Gualdani R, Albertazzi L, Beltram F. Simultaneous intracellular chloride and pH measurements using a GFP-based sensor. Nat Methods. 2010; 7:516–518. [PubMed: 20581829]
55. Collier DM, Snyder PM. Extracellular chloride regulates the epithelial sodium channel. J Biol Chem. 2009; 284:29320–29325. [PubMed: 19713212]
56. Kusama N, Harding AM, Benson CJ. Extracellular chloride modulates the desensitization kinetics of acid-sensing ion channel 1a (ASIC1a). J Biol Chem. 2010; 285:17425–17431. [PubMed: 20385551]
57. Kozak JA, Kerschbaum HH, Cahalan MD. Distinct properties of CRAC and MIC channels in RBL cells. J Gen Physiol. 2002; 120:221–235. [PubMed: 12149283]
58. Kozak JA, Matsushita M, Nairn AC, Cahalan MD. Charge screening by internal pH and polyvalent cations as a mechanism for activation, inhibition, and rundown of TRPM7/MIC channels. J Gen Physiol. 2005; 126:499–514. [PubMed: 16260839]
59. Lee BC, Hong SE, Lim HH, Kim do H, Park CS. Alteration of the transcriptional profile of human embryonic kidney cells by transient overexpression of mouse TRPM7 channels. Int J Exp Cell Physiol. 2011; 27:313–326.
60. Chokshi R, Matsushita M, Kozak JA. Sensitivity of TRPM7 channels to Mg2+ characterized in cell-free patches of Jurkat T lymphocytes. Am J Physiol Cell Physiol. 2012; 302:C1642–C1651. [PubMed: 22460708]
61. Bachhuber T, Konig J, Voelcker T, Murle B, Schreiber R, Kunzelmann K. Cl- interference with the epithelial Na+ channel ENaC. J Biol Chem. 2005; 280:31587–31594. [PubMed: 16027156]
62. Schreiber R, Boucherot A, Murle B, Sun J, Kunzelmann K. Control of epithelial ion transport by Cl- and PDZ proteins. J Memb Biol. 2004; 199:85–98.
63. Baquero Gonzales AF. The regulation of epithelial sodium channels in mammalian taste receptor cells. All Grad Thes Diss Paper. 2009; 418:1–201.
64. Doyon N, Prescott SA, Castonguay A, Godin AG, Kroger H, De Koninck Y. Efficacy of synaptic inhibition depends on multiple, dynamically interacting mechanisms implicated in chloride homeostasis. PLoS Comput Biol. 2011; 7:e1002149. [PubMed: 21931544]
65. Jedlicka P, Deller T, Gutkin BS, Backus KH. Activity-dependent intracellular chloride accumulation and diffusion controls GABA(A) receptor-mediated synaptic transmission. Hippocampus. 2011; 21:885–898. [PubMed: 20575006]
66. Choi DW. Ischemia-induced neuronal apoptosis. Curr Opin Neurobiol. 1996; 6:667–672. [PubMed: 8937832]
67. Pacheco-Alvarez D, Gamba G. WNK3 is a putative chloride-sensing kinase. Int J Exp Cell Physiol Biochem Pharm. 2011; 28:1123–1134.
68. Niisato N, Eaton DC, Marunaka Y. Involvement of cytosolic Cl- in osmoregulation of alpha-ENaC gene expression. Am J Physiol Renal Physiol. 2004; 287:F932–F939. [PubMed: 15292045]
69. Ohsawa R, Miyazaki H, Niisato N, Shiozaki A, Iwasaki Y, Otsuji E, Marunaka Y. Intracellular chloride regulates cell proliferation through the activation of stress-activated protein kinases in MKN28 human gastric cancer cells. J Cell Physiol. 2010; 223:764–770. [PubMed: 20205250]
70. Heimlich G, Cidlowski JA. Selective role of intracellular chloride in the regulation of the intrinsic but not extrinsic pathway of apoptosis in Jurkat T-cells. J Biol Chem. 2006; 281:2232–2241. [PubMed: 16299378]
71. Poulsen KA, Andersen EC, Hansen CF, Klausen TK, Hougaard C, Lambert IH, Hoffmann EK. Deregulation of apoptotic volume decrease and ionic movements in multidrug-resistant tumor cells: role of chloride channels. Am J Physiol Cell Physiol. 2010; 298:C14–C25. [PubMed: 19846756]
72. Paravicini TM, Chubanov V, Gudermann T. TRPM7: a unique channel involved in magnesium homeostasis. Int J Biochem Cell Biol. 2012; 44:1381–1384. [PubMed: 22634382]
73. Liu XH, Chen GG, Vlantis AC, Van Hasselt CA. Iodine mediated mechanisms and thyroid carcinoma. Crit Rev Clin Lab Sci. 2009; 46:302–318. [PubMed: 19958216]

74. Rhoden KJ, Cianchetta S, Duchi S, Romeo G. Fluorescence quantitation of thyrocyte iodide accumulation with the yellow fluorescent protein variant YFP-H148Q/I152L. Anal Biochem. 2008; 373:239–246. [PubMed: 18021945]

75. Yoshida A, Taniguchi S, Hisatome I, Royaux IE, Green ED, Kohn LD, Suzuki K. Pendrin is an iodide-specific apical porter responsible for iodide efflux from thyroid cells. J Clin Endocrinol Metab. 2002; 87:3356–3361. [PubMed: 12107249]

76. Perraud AL, Fleig A, Dunn CA, Bagley LA, Launay P, Schmitz C, Stokes AJ, Zhu Q, Bessman MJ, Penner R, et al. ADP-ribose gating of the calcium-permeable LT RPC2 channel revealed by Nudix motif homology. Nature. 2001; 411:595–599. [PubMed: 11385575]

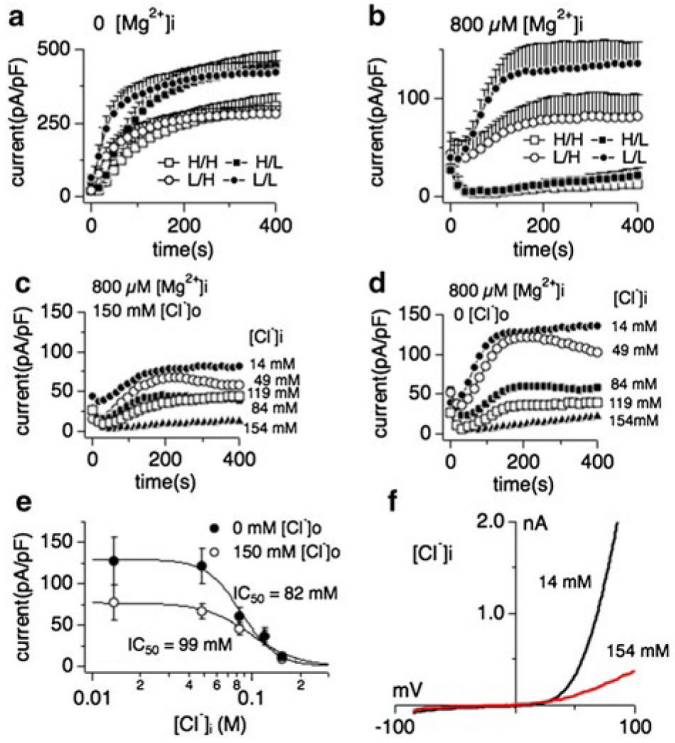

Fig. 1.

Intracellular Mg^{2+} is an obligatory co-factor of chloride-induced TRPM7 inhibition. Whole-cell currents were recorded in HEK293 cell induced to overexpress human TRPM7 (tetHEKTRPM7). Voltage ramps were from −100 to +100 mV over 50 ms time and given at an interval of 2 s. TRPM7 current amplitudes were assessed at +80 mV, averaged and normalized to cell size (in pF). In [H/H] conditions (*open square*), both intracellular and extracellular solutions contained high concentrations of chloride (154 mM each, see "Methods"), either in the form of CsCl (internal) or NaCl (external). In [H/L] conditions (*filled squares*), cells were perfused with high intracellular chloride (154 mM) solution and kept in low extracellular chloride (4 mM) solution (see "Methods"). In [L/H] conditions (*open circles*), cells were perfused with low intracellular chloride (14 mM) solution and high extracellular chloride solution. For [L/L] (*filled circles*), cells were perfused with low chloride both intracellularly and extracellularly. Intracellular free Mg^{2+} was either chelated to 0 mM (*panel a*) or clamped at 800 μM, the latter bringing internal chloride solutions to a total of 14 mM (*panel b*). *Error bars* indicate SEM **a** comparison of effects of intra- and extracellular Cl^- on TRPM7 currents in the absence of intracellular Mg^{2+} (n = 6–8). **b** Comparison of intra- and extracellular Cl^- on TRPM7 currents in the presence of intracellular 800 μM free Mg^{2+} (n = 6–8). **c** Inhibition of TRPM7 currents by increasingly higher intracellular Cl^- concentrations in the presence of high extracellular chloride (154 mM; n = 6–8) and 800 μM intracellular Mg^{2+}. **d** Inhibition of TRPM7 currents by increasingly higher intracellular Cl^- concentration with cells kept in low chloride conditions (4 mM) by substituting NaCl with Na-gluconate. Intracellular Mg^{2+} was kept at 800 μM. **e** Dose–response curves for TRPM7 inhibition by increasing intracellular Cl^- concentrations from data in panels C and D. Data points correspond to averaged, cell-size (in pF) normalized current amplitudes measured at +80 mV and at 200 s of whole-cell recording and plotted as a function of Cl^- concentration (n = 6–8 each data point). The best fit was obtained by a Hill coefficient close to 3 and was therefore fixed at that value. The calculated

IC_{50} value for Cl^--induced inhibition of TRPM7 currents with or without external Cl^- is IC_{50} = 99 ± 9 mM (*open circles*) and 82 ± 6 mM (*solid circles*), respectively. Note the overall larger current under low external Cl^- conditions. **h** Representative current voltage (I/V) relationships for TRPM7 in the presence of intracellular 14 or 154 mM Cl^- taken from *panel c*

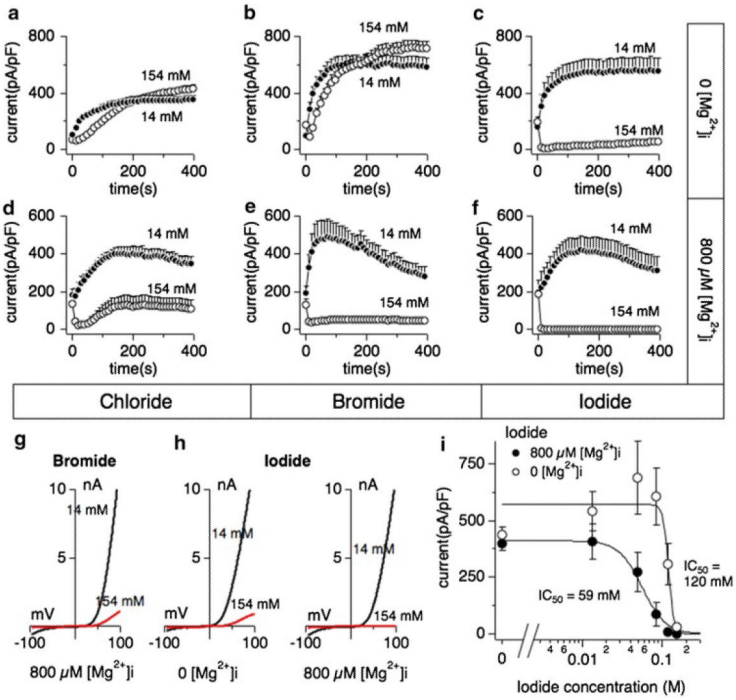

Fig. 2.

Iodide inhibits human TRPM7 currents independently of intracellular Mg^{2+}. Whole-cell patch clamp experiments were performed in tetHEKTRPM7 cells. Voltage ramps were from −100 to +100 mV over 50 ms and given at an interval of 2 s. TRPM7 current amplitudes were assessed at +80 mV, averaged and normalized to cell size (in pF). *Error bars* indicate SEM. For detailed solution composition see "Methods". **a** TRPM7 currents measured in cells perfused with either 14 mM (*solid circles*) or 154 mM (*open circles*) intracellular Cl^- solution in the absence of intracellular Mg^{2+} (n = 6–8). **b** TRPM7 currents in cells perfused with either 14 mM (*solid circles*) or 154 mM (*open circles*) intracellular bromide (Br^-) solution in the absence of Mg^{2+} (n = 6–8). **c** TRPM7 currents in cells perfused with either 14 mM (*solid circles*) or 154 mM (*open circles*) intracellular iodide (I^-) solution in the absence of Mg^{2+} (n = 6–8). **d** TRPM7 current development in the presence of 800 μM Mg^{2+} and either 14 mM (*solid circles*) or 154 mM (*open circles*) intracellular Cl^- (n = 6–8). **e** TRPM7 currents in 14 or 154 mM intracellular Br^- and 800 μM Mg^{2+} (n = 6–8). **f** TRPM7 currents in 14 or 154 mM intracellular I^- and 800 μM Mg^{2+} (n = 6–8). **g** Representative I/V curve for TRPM7 with intracellular 14 mM (*black trace*) or 154 mM Br^- (*red trace*) in the experiments described in *panel e*. **h** Representative I/V relationships for TRPM7 with 14 mM (*black trace*) or 154 mM (*red trace*) intracellular I^- solution in the experiments described in *panel c* and *panel f*, respectively. All I/V curves were extracted at 200 s experimental time. **i** Dose–response curves for TRPM7 inhibition by increased I^- concentrations in the absence (*open circles*) or presence (*solid circles*) of intracellular 800 μM Mg^{2+}. Data points correspond to average current amplitudes measured at +80 mV at 200 s of whole cell recording, normalized to cell size and plotted as a function of internal I^- concentration (n = 6–8). The best fit was obtained by a Hill coefficient close to −4 and −13 for the responses with intracellular 800 μM Mg^{2+} (*solid circles*) or without intracellular Mg^{2+} (*open circles*), respectively. Therefore the coefficients were fixed at those values, respectively. With intracellular Mg^{2+}, the calculated IC_{50} value for I^--induced inhibition of TRPM7 currents is 59 ± 1 mM, and 120 ± 6 mM without Mg^{2+}

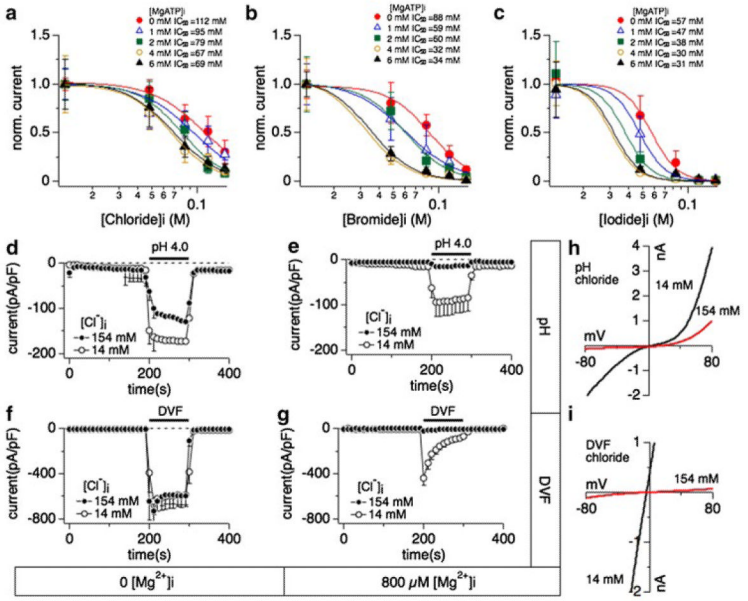

Fig. 3.

Relationship between halide-induced inhibition of TRPM7 and intracellular Mg·ATP, extracellular divalent-free- or acidic pH conditions. Whole-cell patch clamp experiments were performed in tetHEKTRPM7 cells. Voltage ramps were from −100 to +100 mV over 50 ms and acquired at 0.5 Hz. TRPM7 current amplitudes were assessed at +80 mV, averaged and normalized to cell size (in pF). *Error bar* indicates SEM. For detailed solution composition see "Methods". **a** Dose–response curves of TRPM7 established as a function of increasing intracellular chloride concentrations and at various fixed intracellular Mg·AT P. Each dose–response curve was calculated as in Fig. 1e and normalized to 1 by dividing with Y_{max} (n = 4–8). All the Hill coefficients of the dose–response curves were fixed to −3. **b** Dose–response curves of TRPM7 plotted as a function of intracellular bromide concentration at various fixed Mg·ATP. Each dose–response curve was calculated as in Fig. 1e and normalized to 1 by dividing with Y_{max} (n = 4–8). Hill coefficients were fixed to −3. **c** Comparison of dose–response curves as a function of iodide concentrations at different fixed Mg·ATP. Each dose–response curve was calculated as in Fig. 1e and normalized to 1 by dividing with Y_{max} (n = 4–8). Best-fit Hill coefficients approximated −5 and were therefore fixed to −5. **d** Effects of external acidic solution (pH 4.0) on TRPM7 inward currents when perfusing cells with intracellular solution containing either 14 mM (*open circles*) or 154 mM (*solid circles*) Cl^-. Intracellular Mg^{2+} was chelated to zero mM by adding 10 mM EDTA (n = 6–8). The *black bar* indicates application time from 200 to 300 s. **e** Effects of external acidification (pH 4.0) on TRPM7 inward current while perfusing cells with internal solution containing 14 mM (*open circles*) or 154 mM (*solid circles*) Cl^-. Intracellular Mg^{2+} was clamped to 800 μM (n = 6–8). **f** Application of divalent-free external solution (DVF) on fully developed TRPM7 currents assessed at −80 mV and cells perfused with internal solution containing either 14 mM (*open circles*) or 154 mM (*solid circles*) Cl^-. Intracellular Mg^{2+} was chelated to close to 0 mM by adding 10 mM EDTA (n = 6–8). **g** Application of a DVF solution on TRPM7 inward currents assessed at −80 mV where cells were perfused with internal solution containing either 14 or 154 mM Cl^-. Intracellular Mg2+ was clamped to 800 μM (n = 6–8). **h** Representative I/V relationships for TRPM7 currents assessed in the presence of intracellular 14 mM (*black trace*) Cl^- or 154 mM (*red trace*) Cl^- in response to acidic pH as shown in *panel e*. All I/V curves were extracted at 210 s into the experiment. **g** Representative I/V curves for TRPM7 in the presence of intracellular 14 mM (*black trace*)

Cl^- and 154 mM (*red trace*) Cl^- in response to DVF conditions as described in *panel g*. All I/V curves were extracted at 210 s into the experiment

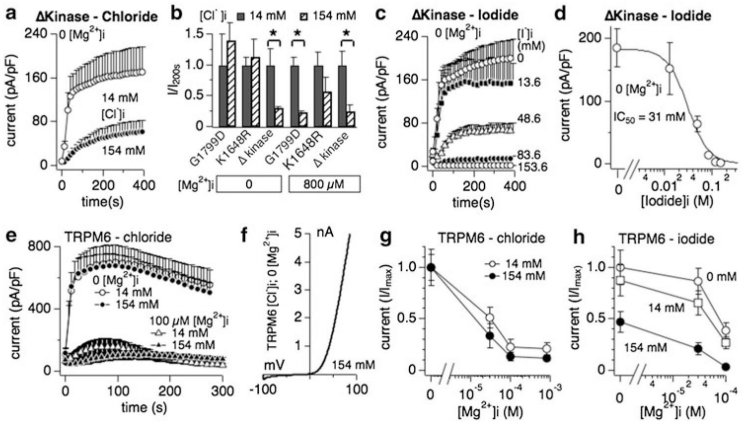

Fig. 4.

Interaction of halides with TRPM7 delta kinase channels and TRPM6. **a** Whole-cell patch clamp experiments in tetracycl-ininducible HEK293 cells overexpressing TRPM7 truncated kinase mutant (Δkinase) [7]. Cells were perfused with intracellular solution containing either 14 mM or 154 mM Cl^- and in the absence of intracellular Mg^{2+} (n = 6–8). See "Methods" for solution details. All currents were assessed at +80 mV during a voltage-ramp stimulus ranging from −100 to +100 mV over 50 ms and given at 0.5-Hz intervals. Currents were averaged and normalized to the cell capacitance (in pF) recorded at whole-cell break-in. *Error bars* indicated SEM. **b** The bar graph analysis shows normalized current amplitudes measured at +80 mV and at 200 s for three different TRPM7 kinase domain mutants (G1799D, K1648R and Δkinase) and normalized as $I/I_{max(200s)}$. Internal solutions were kept at low (14 mM, *black bars*) or high (154 mM, *diagonally striped bars*) chloride and were supplemented with 800 μM $[Mg^{2+}]_i$ or not as indicated in the graph. **c** Inhibition of TRPM7 Δkinase currents by increasing intracellular I^- concentrations in the absence of intracellular Mg^{2+} (n = 6–8). **d** Dose–response curve analysis of TRPM7 currents shown in *panel c*. Data points correspond to average current amplitudes measured at +80 mV at 200 s of whole-cell recording, plotted as a function of I^- concentration from *panel c* (n = 6–8). The best fit was obtained by a Hill coefficient close to −3 and was therefore fixed at that value. The calculated IC_{50} value for I^--induced inhibition of TRPM7 Δkinase currents is IC_{50} = 31 ± 3 mM. **e** Assessment of chloride inhibition on human TRPM6 (hTRPM6) transiently expressed between 26 and 30 h in wild-type HEK293 cells (see "Methods"). Currents were elicited by standard voltage ramps, assessed at +80 mV, averaged, normalized for cell size (in pF) and plotted versus time of the experiment. **f** Representative I/V curve for TRPM6 in the presence of intracellular 154 mM Cl^- and without internal Mg^{2+}, taken from experiments in *panel e*. All I/V relationships were taken at 75 s and were derived from a high-resolution current record in response to a voltage ramp of 50 ms duration that ranged from −100 to +100 mV. **g** Cells transiently expressing hTRPM6 were perfused with internal solutions containing either 14 or 154 mM Cl^- and increasing intracellular Mg^{2+} concentrations. Data shown were measured at +80 mV, assessed at 75 s whole-cell time and normalized to I/I_{max} (n = 6–8). **h** Dose-dependent inhibition of hTRPM6 currents plotted as a function of Mg^{2+} concentrations assessed at different fixed I^- concentrations. Data points correspond to average current amplitudes measured at +80 mV and 75 s of whole cell recording (n = 4–8). Data were normalized to I/I_{max}

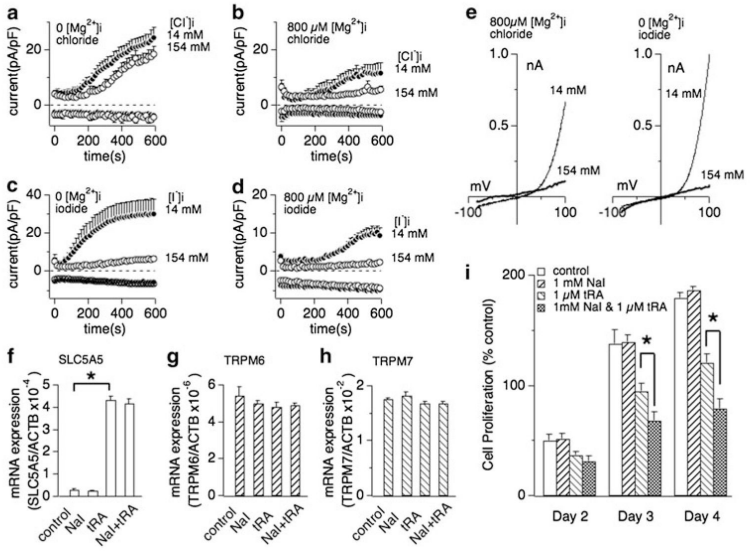

Fig. 5.

Extracellular iodide suppresses breast cancer cell proliferation in dependence of SLC5A5 sodium-iodide symporter expression. **a** Whole cell currents were recorded in MCF-7 breast cancer cells and normalized to cell capacitance (in pF). Cells were perfused with 14 or 154 mM Cl^- in the absence of intracellular Mg^{2+} (n = 6–8). **b** Cells were perfused with 14 or 154 mM Cl^- in the presence of 800 μM free Mg^{2+} in the internal solution (n = 6–8). **c** Low (14 mM) or high (154 mM) iodide perfusion of MCF-7 in the absence of intracellular Mg^{2+} (n = 6–8). **d** Low (14 mM) or high (154 mM) iodide perfusion of MCF-7 with additional 800 μM free Mg^{2+} (n = 6–8). **e** Representative current voltage (I/V) curves for native TRPM7 currents in MCF-7 cells in the presence of intracellular 14 and 154 mM halide ions (Cl^- or I^-) described in *panel b* or *panel c*, respectively. All I/V curves were extracted at 600 s whole-cell time and were derived from a high-resolution current record in response to a voltage ramp of 50 ms ranging from −100 to +100 mV. **f, g, h** Changes of mRNA expression of SLC5A5 (sodium-iodide symporter, *panel f*), TRPM6 (*panel g*) and TRPM7 (*panel h*) by treatment of 1 mM sodium iodide (NaI), 1 μM trans-retinoic acid (tRA) or a combination thereof. The expression of each mRNA is normalized to β-actin expression. Data are mean ± SEM from three independent experiments. Note that exposure of MCF-7 cells to 1 μM tRA, but not 1 mM NaI, significantly increases SLC5A5 mRNA expression. The same treatment had no significant effect on TRPM6 (*panel g*) or TRPM7 mRNA expression (*panel h*). **i** Effect of NaI on MCF-7 breast cancer cell proliferation. The histogram shows the mean number of viable MCF-7 cells counted on the 2nd, 3rd and 4th day after cell seeding. Cells were planted at a density of 1.5×10^5 ml^{-1} with the medium containing 10 % FBS. The cells were then treated with medium vehicle (control), 1 μM tRA, 1 mM NaI or 1 μM tRA and 1 mM NaI combined (n = 4 independent experiments). *Error bars* indicate SEM. *Star* indicates $P < 0.002$

Table 1

Composition of bath solution (in mM)

	High $[Cl^-]_o$	Low $[Cl^-]_o$
NaCl	150	
Na-gluconate		150
HEPES	10	10
$CaCl_2$	1	1
$MgCl_2$	1	1
Glucose	10	10

Table 2

Composition of pipette solution (in mM)

	0 Mg (low $[Cl^-]_i$)	0 Mg (high $[Cl^-]_i$)	0.8 Mg (low $[Cl^-]_i$)	0.8 Mg (high $[Cl^-]_i$)
CsCl	10	150	10	150
Cs-glutamate	140		140	
HEPES	10	10	10	10
$MgCl_2$			1.8	1.8
EDTA	10	10	1	1
EGTA			1	1

Table 3

Composition of pipette solution for various Cl^- concentration (in mM)

	14 $[Cl^-]_i$	**49 $[Cl^-]_i$**	**84 $[Cl^-]_i$**	**119 $[Cl^-]_i$**	**154 $[Cl^-]_i$**
CsCl	10	45	80	115	150
Cs-glutamate	140	105	70	35	0
HEPES	10	10	10	10	10
$MgCl_2$	1.8	1.8	1.8	1.8	1.8
EDTA	1	1	1	1	1
EGTA	1	1	1	1	1

Table 4

Liquid junction potential (in mV) for external and internal halide concentrations

	Liquid junction $[Cl^-]_o$		Liquid junction (mV)	$[Cl^-]_i$, $[Br^-]_i$ or $[I^-]_i$ (mM)
	High $[Cl^-]_o$ (mV)	Low $[Cl^-]_o$ (mV)		
0 Mg (low $[Cl^-]_i$)	5.9	−1.0	7.3	13.6
0 Mg (high $[Cl^-]_i$)	−1.9	−11.3	5.3	48.6
0.8 mM Mg^{2+} (low $[Cl^-]_i$)	7.3	−2.4	3.2	83.6
0.8 mM Mg^{2+} (high $[Cl^-]_i$)	−0.9	−10.5	1.2 −0.9	118.6 153.6